Peer-reviewed version available at Appl. Sci. 2018, 9, 16; doi:10.3390/app9010016

*Article*

# Efficient Photoelectrochemical Water Splitting Reaction using Electrodeposited $Co_3Se_4$ Catalyst

**Yelyn Sim‡, Jude John‡, Subramani Surendran‡, Byeolee Moon, and Uk Sim***

Department of Materials Science & Engineering, Chonnam National University, Gwangju 61186, Republic of Korea

* Correspondence: usim@jnu.ac.kr ; Tel.: +82-62-530-1718

‡ These authors contributed equally to this work.

## Abstract

Photoelectrochemical water splitting is a promising field for sustainable energy production using hydrogen. Development of efficient catalysts is essential for resourceful hydrogen production. The most efficient catalysts reported to date have been extremely precious rare-earth metals. One of the biggest hurdles in this research area is the difficulty of developing highly efficient catalysts comparable to the noble metal catalysts. Here, we report that non-noble metal dichalcogenide ($Co_3Se_4$) catalysts made using a facile one-pot electrodeposition method, showed highly efficient photoelectrochemical activity on a Si photocathode. To enhance light collection and enlarge its surface area even further, we implemented surface nano-structuring on the Si surface. The nano-structured Si photoelectrode has an effective area greater than that of planar silicon and a wider absorption spectrum. Consequently, this approach exhibits reduced overvoltage as well as increased photo-catalytic activity. Such results show the importance of controlling the optimized interface between the surface structure of the photoelectrode and the electrodeposited co-catalyst on it to improve catalytic activity. This should enable other electrochemical reactions in a variety of energy conversion systems.

**Keywords:** Photoelectrochemical cell; hydrogen evolution reaction (HER); metal free catalyst; Cobalt selenide catalyst

## 1. Introduction

Increasing energy demand and the rapid depletion of fossil fuels have made it inevitable that renewable sources of alternative energy be found.[1] Despite the difficulties of finding alternative sources of energy, hydrogen has emerged as an excellent source of clean energy that could serve as a key technology for providing alternative energy.[2] The state-of-the-art high-efficiency hydrogen-producing catalysts are based on noble metals like Pt.[3] However, the cost and scarcity of noble metals are preventing hydrogen energy from being used in a variety of applications. Moreover, depletion of fossil fuels at a steady pace is contributing to the emerging energy crisis.[4] In this situation, hydrogen has become attractive as an excellent option for clean energy that could also serve as a key technology in providing sustainable alternative energy.[5] The discovery of photoelectrochemical water splitting using $TiO_2$ by Honda and Fujishima in 1972 has completely revolutionized the area of photoelectrochemical water splitting using semiconductor photoelectrodes.[6] In this regard, photoelectrochemical (PEC) water splitting to produce hydrogen is turning out to be a promising strategy through which energy produced from solar irradiation could be transformed and stored in the form of hydrogen.[2, 7]

Photoelectrodes provide the essential function of converting solar energy-to-fuel. To achieve this conversion, the photoelectrode should possess a reasonable band gap for absorption of the incoming incident light. This is necessary to drive the reaction for the reduction and oxidation of water. The desired photoelectrode also has to provide charge transfer kinetics fast enough to minimize the recombination of oppositely charged ions at the electrode/electrolyte interface.[7] Metal oxides have larger bandgaps (higher than 2 eV) which restrains their light absorption capability and thereby makes them inefficient for solar energy conversion.[8-10] Among the various semiconductor materials that have been researched, p-type silicon (Si) stands out as a well-known photocathode owing to its excellent photoelectrochemical water splitting properties.[11-14] Silicon is also an Earth-abundant semiconductor material with a narrow bandgap (1.12 eV). These qualities make it an appropriate material for absorbing a larger portion of the solar spectrum, and thus an ideal candidate for the photovoltaic industry.[15] Even with these advantages, Si is quite unstable in aqueous conditions and in the absence of a catalyst, the reaction at the p-Si/electrolyte interface results in sluggish kinetics at zero overpotential (i.e., 0 V vs RHE).[16]

One strategy to overcome this was to incorporate a corrosion-resistant protective layer that would minimize inhibition of the photogenerated carriers and thereby improve the charge transfer. Numerous studies have been carried out in the area of adding protective layers to Si photoelectrodes to improve the stability of p-Si photoelectrodes in aqueous conditions.[17-19] Platinum (Pt)[20] is well known for its use as an electrocatalyst in PEC hydrogen production. It is however, also a precious metal, the scarcity of which makes its large-scale deployment for PEC water splitting rather unlikely.

In response to these conditions, tremendous effort has been expended to find and develop Earth-abundant non-precious catalysts for hydrogen production.

Recently, first-row transition-metal dichalcogenides have emerged as significant prospects for use in water-splitting reactions, and been proposed as replacements for precious metals (i.e., Pt). This proposal is especially compelling due to their natural-abundance and high catalytic activity. Among these options, $CoX_2$ (X = S, Se) has lower overpotential with smaller Tafel slope and large exchange current, and variants have shown promising development in HER reactions.[21-23] Yu et al. established that higher catalytic rendition could be achieved by turning bulk $CoSe_2$ into an ultrathin nanosheet and thereby significantly enhancing the surface-to-volume ratio due to the vacancy rich surfaces.[24-25] Similarly Zhang et al. found that by a phase engineering process, they were able to produce more edge sites on $CoSe_2$ catalyst. This included polymorphic phases of $CoSe_2$ that were obtained through a temperature controlled process for calcination of amorphous $CoSe_x$. Their work demonstrated that the grain boundaries existing between the two phases would unravel new HER active sites, thereby enhancing the overall HER activity in $CoSe_2$.[26]

However, regarding actual development of HER photocathodes, relatively few catalysts have been successfully integrated into these photocathodes. Moreover, many of these could not achieve their full potential due to the lack of effective interfacing of these active nanosized HER catalysts with the silicon photoabsorbers.[27-29] In the light of these developments, we report a simple and facile method for electrodeposition of $Co_3Se_4$ as a co-catalyst passivation-layer onto a p-Si photocathode to enhance the photoelectrochemical water-splitting reaction. To provide better substrate selectivity, the catalytic activity of the $Co_3Se_4$ co-catalyst was tested using Fluorine-doped Tin Oxide (FTO) and a glassy carbon electrode as substrates. The $Co_3Se_4$ decorated onto the FTO substrate exhibited excellent HER ($\eta_{(10)}$ = 215 mV) and OER ($\eta_{(4)}$ = 562 mV) catalytic activity. The resulting low Tafel value (42.5) and 103 mV/dec occurred under pH 0 and pH 8 conditions, respectively. Hence, new $Co_3Se_4$ electrocatalysts with optimized working electrode selectivity and controlled deposition rate are proposed as an efficient new bi-functional catalyst for water-splitting applications.

## 2. Materials and Methods

**2.1 Materials**. Sodium selenite ($Na_2SeO_3$), cobalt acetate ($Co(CH_3COO)_2$), lithium chloride (LiCl), perchloric acid ($HClO_4$), silver nitrate ($AgNO_3$), hydrochloric acid (HCl), nitric acid ($HNO_3$), and hydrofluoric acid (HF) were purchased from Sigma Aldrich (Seoul, Rep. of Korea, 2018). All reagents used in this work were of analytical grade purity and were used without further purification. As (photo)electrodes, Si substrates (B-doped, p-type, 500 μm thickness, 10–15 Ω·cm resistivity, (100)

oriented) were purchased from Namkang Inc. (Seongnam, Rep.of Korea, 2018) and FTO glass slides (1 x 2 $cm^2$, 7 Ω/sq resistivity) were purchased from Wooyang GMS (Namyangju, Rep. of Korea, 2018). Si wafers were cut to dimensions of 8 x 8 $mm^2$ and then each of these Si wafers was cleaned prior to deposition with acetone, 2-propanol, and deionized water, respectively, using a bath sonicator (10 min each). In the chemical etching of the nanostructured Si (NSi) surface, the Si substrates were dipped into a solution containing 20 mL aqueous etchant solution of $AgNO_3$ (0.679 g, 0.02 M) and HF (5 M) under ambient conditions (25 °C). Finally, Ag residue was completely removed from the nanostructured silicon surface by treating with 70% nitric acid solution for two hours.

**2.2 Electrodeposition of $Co_3Se_4$.** Prior to electrodeposition, the substrates were cleaned following a standard protocol. For electrodeposition, substrates of planar silicon, nanostructured Si (NSi), and FTO were used to get the best possible results from the three electrodes. An aqueous solution containing 20mM $Na_2SeO_3$ (0.101 g), 20 mM $Co(CH_3COO)_2$ (0.146 g) and 100 mM LiCl (0.0121 g) were placed in a 30 mL container. The solution was kept near pH 2 by adding dilute HCl. The deposition was conducted at room temperature in a single compartment glass cell using a three-electrode configuration. Electrodeposition was performed with a CHI 7008E (CH Instruments, Inc., Austin, TX, USA, 2018) potentiostat. Graphite rod was used as a counter electrode and Ag/AgCl (3M NaCl) was used as the reference electrode for the electrodeposition. The chronoamperometric deposition was conducted at −0.8 V for varying deposition times (5, 10, or 15 s), and we determined that the optimal time was 15 s. A thin film of $Co_3Se_4$ co-catalyst was formed on the surface of the working electrodes.

**2.3 Photoelectrochemical measurements.** Photoelectrochemical tests were conducted using a three-electrode cell. Working electrodes comprising a planar silicon photoelectrode, nanowire structured silicon photoelectrode, and FTO glass were used. Graphite rods were used as counter electrodes and Ag/AgCl (3M NaCl) as reference electrodes. Each reference electrode was calibrated to −0.201 V (vs RHE) in a proton-rich aqueous solution of 1 M perchloric acid, and purged with a high-purity saturated $H_2$ at 25 °C. For solar irradiation, a 300 W Xenon lamp was used as the light source at a light intensity of 100 mW/$cm^2$ (Air Mass 1.5 Global condition glass filter).

## 3. Results and Discussion

Cobalt selenide ($Co_3Se_4$) was deposited electrochemically onto conductive electrodes by the electrodeposition method. The X-ray diffraction (XRD) pattern shown in **Figure 1** reveals highly intense and crystalline peaks of prepared cobalt selenide sample. The peaks confirm the single-phase formation of pure monoclinic crystal system of $Co_3Se_4$, which exactly corresponds with the standard JCPDS card No. 98-009-9990. The prepared $Co_3Se_4$ was in well agreement with the lattice parameters

of space group of P21/c (space group number 14). Scanning electron microscopy (SEM) measurements were employed to confirm the morphology of the $Co_3Se_4$ film, as shown in Figure 1 (a). The nanoporous structure of the $Co_3Se_4$ catalyst was confirmed from the corresponding top-view and cross-sectional view SEM images. To determine the elemental composition of the film, energy dispersive spectrometry (EDS) was performed (Figure 1 (b)). To clarify this further, transmission electron microscopy (TEM) measurements of the deposited film were conducted, as shown in Figure 1 (c). Information about the lattice fringe with an inter-planar spacing of 2.67 nm, revealed that the electro-deposited $Co_3Se_4$ film strongly corresponds to the (111) plane of the obtained XRD pattern.

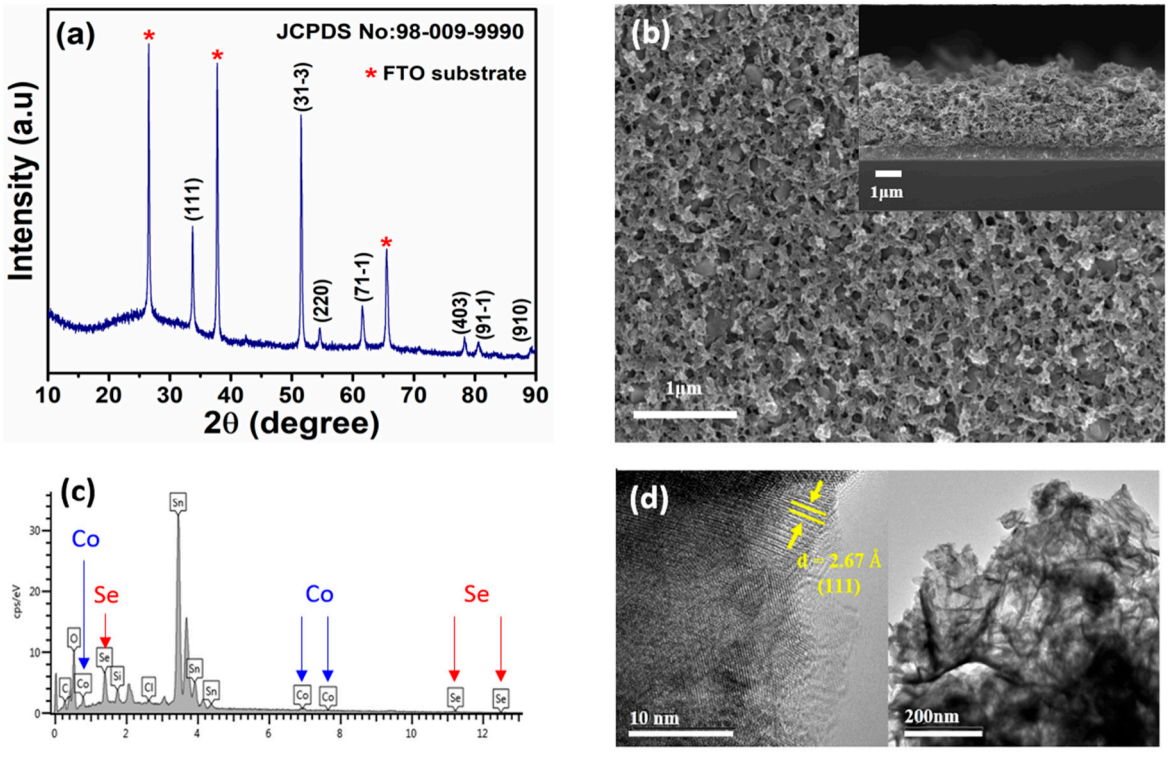


**Figure 1. Surface characterization of the cobalt selenide film:** (a) XRD pattern of $Co_3Se_4$, (b) Scanning electron microscopy (SEM) images of $Co_3Se_4$ electrodeposited on FTO, (c) Energy dispersive spectrometry (EDS) spectrum showing the presence of cobalt and selenide elements, and (d) Transmission electron microscopy (TEM) image to identify $Co_3Se_4$.

Photoelectrochemical measurements indicated that the electrodeposited $Co_3Se_4$ film on the photoelectrode acted as an effective layer for the hydrogen evolution reaction (HER). Figure 2a shows the resulting photoresponse of bare planar Si and $Co_3Se_4$ on planar Si. In the case of $Co_3Se_4$ on planar Si, the current density started to increase negatively much earlier than that of bare planar Si. This indicates that the $Co_3Se_4$/Si system has higher onset potential, defined as the specific potential at −1 mA/cm$^2$. The onset potential ($V_{os}$) of $Co_3Se_4$/Si ($V_{os}$ = 0.216 V vs. RHE at −1 mA/cm$^2$) is 303 mV higher than that of planar Si ($V_{os}$ = −0.087 V vs. RHE at −1 mA/cm$^2$). The potential vs current plot under dark condition shows a 1 μA/cm$^2$ scale of current density, which indicates that the photoresponse of the

$Co_3Se_4$/Si cell operated well with and without illumination. However, when $Co_3Se_4$ was deposited on the Si electrode, the saturation current density decreased by approximately 23% from the initial current density (from −34.1 to −26.4 mA/cm$^2$). This was attributed to the reduced light collection caused by deposition of the semi-transparent $Co_3Se_4$ film. To evaluate the photocathodic efficiency, a half solar-to-hydrogen conversion efficiency was introduced. It was defined as [(photocurrent density at the reversible potential (0 V vs. RHE), $J_{V=0}$ (mA/cm$^2$) × (open circuit potential, $V_{oc}$ (V) × Fill Factor / 100 (mW/cm$^2$) × 100 (%)].[2, 30] The equation is also equal to a maximum value of [$J_{ph}$ (mA/cm$^2$) × ($V_{redox}$-$V_b$) (V)/ ($P_{light}$ (mW/cm$^2$) × 100 %)].[2, 30] Herein, $J_{ph}$ is the photocurrent density obtained under the applied bias $V_b$, and $V_{redox}$ is the redox potential for hydrogen production (0 V vs. RHE). $V_{bias}$ is an externally applied bias potential often necessary to achieve reasonable photocurrents, and $P_{light}$ is the intensity of the incident light under AM 1.5 G conditions. In this work, the incident light intensity was maintained at 100 mW/cm$^2$. From calculation, the half solar-to-hydrogen conversion efficiency increased to 10-times higher than for bare planar Si. Consequently, it was determined that $Co_3Se_4$ is a highly active film for photoelectrochemical hydrogen production in terms of photocathodic efficiency.

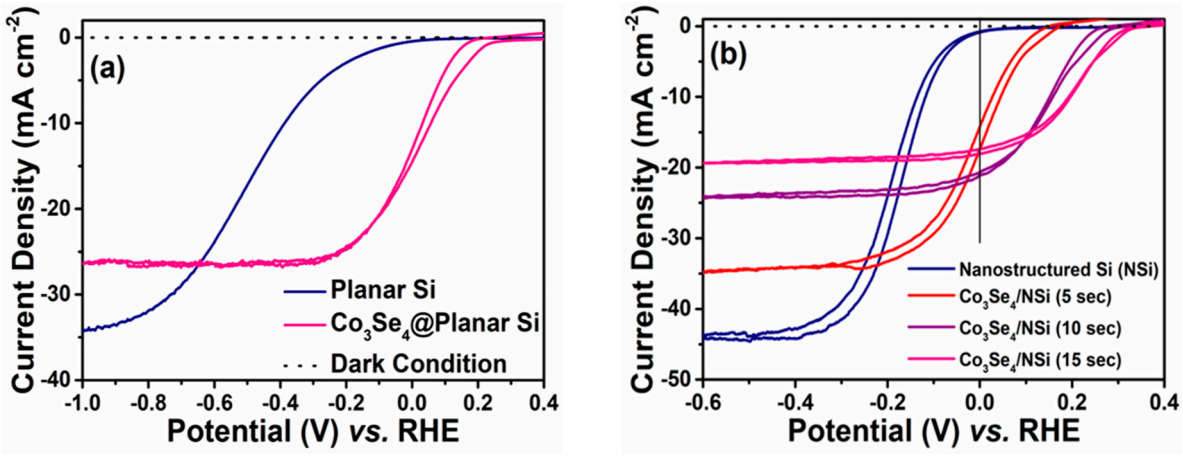


**Figure 2. Cyclic voltammograms of electrodeposited cobalt selenide ($Co_3Se_4$) on Si photocathodes:** (a) Current density-potential (*J-E*) curves of bare planar Si photoelectrode and $Co_3Se_4$ electrodeposited with $Co_3Se_4$ under dark condition and light condition, respectively, (b) Photoresponse current density-potential curves for bare planar Si and $Co_3Se_4$ deposited planar Si, (c) Photocurrent density-potential (J-E) curve according to cobalt selenide electrodeposition time.

Treatment of the nanostructured Si surface using a metal-catalyzed electroless etching process further increased the light-to-hydrogen conversion efficiency. Optimized nanostructuring of the Si electrode surface increased the limiting current density (the saturation current density at high negative potential) to 44.0 mA/cm$^2$. This is 1.29 times higher than that of bare planar Si (34.1 mA/cm$^2$), as shown in Figure 2 (a) and (b). The $V_{os}$ of the nanostructured Si (−0.007 V vs. RHE) also shifted by

a positive 80 mV ($V_{os}$ of bare planar Si: −0.087 V vs. RHE). Consequently, the conversion efficiency of the nanostructured Si photocathode (0.04%) increased two fold compared to that of bare planar Si (0.02%). The enhanced efficiency of the nanostructured photoelectrode surface is mainly attributed to increased effective surface area and reduced reflectance of incident light. To increase the photocathodic activity even more, $Co_3Se_4$ was deposited electrochemically as a function of time, maintaining the applied potential of −0.8 V vs. RHE. Figure 2 (b) shows representative photoresponse results with various electrodeposition times. With increasing deposition time, the onset potential shifted positively (anodically) while the limiting current density continuously decreased, induced by deposition of much thicker $Co_3Se_4$ film. Overall, the conversion efficiency increased and conversion became saturated at 15 sec of electrodeposition time. The efficiency of the $Co_3Se_4$/nanostructured Si with 15 s of electrodeposition was 2.71%, a value 136 times higher than that of bare planar Si and 68 times higher than bare nanostructured Si without co-catalyst. From these results, it was shown that an optimal thickness of $Co_3Se_4$ co-catalyst film exists for efficient hydrogen production.

**Table 1 Half solar-to-hydrogen conversion efficiency of various photocathodes**

| Type of Si photocathode | Efficiency (%) |
|---|---|
| Planar Si | 0.02 |
| $Co_3Se_4$ on planar Si | 0.20 |
| Nanostructured Si | 0.04 |
| $Co_3Se_4$ on nanostructured Si (5 s) | 0.47 |
| $Co_3Se_4$ on nanostructured Si (10 s) | 1.72 |
| $Co_3Se_4$ on nanostructured Si (15 s) | 2.71 |

To evaluate the electrocatalytic properties of the material, the HER electrocatalytic activity was examined using the customary three-electrode system. To understand better the electrocatalytic activity with respect to the substrate, the $Co_3Se_4$ material was deposited on a glassy carbon electrode (GCE) and on a fluorine-doped tin oxide (FTO) substrate. In Figure 2 (a), the HER polarization curves of $Co_3Se_4$ on FTO and GC electrodes are compared, along with those of bare FTO and bare GCE. In all the polarization curves, the reductive current density started to increase negatively according to the cathodic potential applied, and promoted the hydrogen evolution reaction (HER). The HER curves indicate that $Co_3Se_4$(10) on the FTO electrode exhibited superior onset potential (−0.189 V vs. RHE at −1 mA/cm$^2$) than did $Co_3Se_4$(10) deposited on GCE (−0.192 V vs RHE at −1 mA/cm$^2$) and better onset potential than did bare FTO (−0.552 V vs RHE at −1 mA/cm$^2$) and GC (−0.644 V vs RHE at −1 mA/cm$^2$) electrodes. Moreover, at a similar current density of 5 mA/cm$^2$, the $Co_3Se_4$ deposited on the FTO conductive electrode showed enhanced electrocatalytic activity resulting in a lower overpotential of 239 mV compared to $Co_3Se_4$ on the GC electrode (292 mV). This indicated that FTO

is a more suitable substrate and improves catalytic activity. Therefore, in-depth analyses were carried out at various deposition times of the $Co_3Se_4$ electrocatalysts on the FTO substrate. Figure 2 (b) shows that the HER activity of the $Co_3Se_4$ electrocatalyst varies with respect to the deposition time (5–25 s). The electrocatalytic activity of the time dependent $Co_3Se_4$ catalysts was observed to increase gradually with deposition time from 5 to 20 s, exhibiting a very low onset potential (−0.205 V to −0.119 V vs. RHE at −1 mA/cm$^2$). Subsequently, the sample deposited for 25 s abruptly declined due to an increase in onset potential (−0.152 V vs. RHE at −1 mA/cm$^2$) compared to the sample deposited for 20 s. Figure 2c sorts out the overpotential demanded by prepared $Co_3Se_4$ electrocatalysts deposited on the FTO for different times. The enhanced HER catalytic activity of the $Co_3Se_4$ (20 s) catalysts can be attributed to better quality loading of the catalyst on the FTO substrate. However, the decrease in the activity of the $Co_3Se_4$ (25 s) catalysts may be due to overloading of the catalysts on the FTO. This clumps the electroactive sites, resulting in a poor interface between electrode and electrolyte. Therefore, controlled loading of the catalysts over the substrates plays a vital role because it tends to generate more electroactive sites, which facilitates superior electrocatalytic activity. Overall, the $Co_3Se_4$ catalysts deposited on the FTO substrate for 20 s delivered superior HER electrocatalytic activity by requiring only a very low overpotential of 215 mV to acquire an improved current density of 10 mA/cm$^2$. This overpotential (215 mV) required by the $Co_3Se_4$ catalysts electrodeposited on the FTO substrate for 20 s seems very efficient compared to the previously reported results on metal selenides.

To gain additional and more detailed information about the inherent properties of the electrodeposited $Co_3Se_4$, the current density vs potential curves of the $Co_3Se_4$ samples on GC and on FTO were converted to Tafel plots to study the rate limiting step of the HER reaction. First, the Tafel slopes shown in Figure 2d were calculated to be 66.2 and 42.5 mV/dec for $Co_3Se_4$ on GC and on FTO, respectively. The $Co_3Se_4$(20) electrocatalyst deposited on FTO yielded a consistently low Tafel value, substantiating the upgraded electrocatalytic activity of the material. This provided further evidence that hydrogen can be generated by a Heyrovsky reaction mechanism, by which one proton adsorbs to the electrode and one hydrated proton comes from the electrolyte (and they combine) to make hydrogen gas. The exchange current density of $Co_3Se_4$ on GC was $1.62\times10^{-6}$ A/cm$^2$ and that of $Co_3Se_4$ on FTO was $4.47\times10^{-8}$ A/cm$^2$, which values were derived from the results on variation in the substrate condition. In conclusion, electrodeposited $Co_3Se_4$(20) showed an effective hydrogen evolution mechanism with any of the conductive standard electrodes.

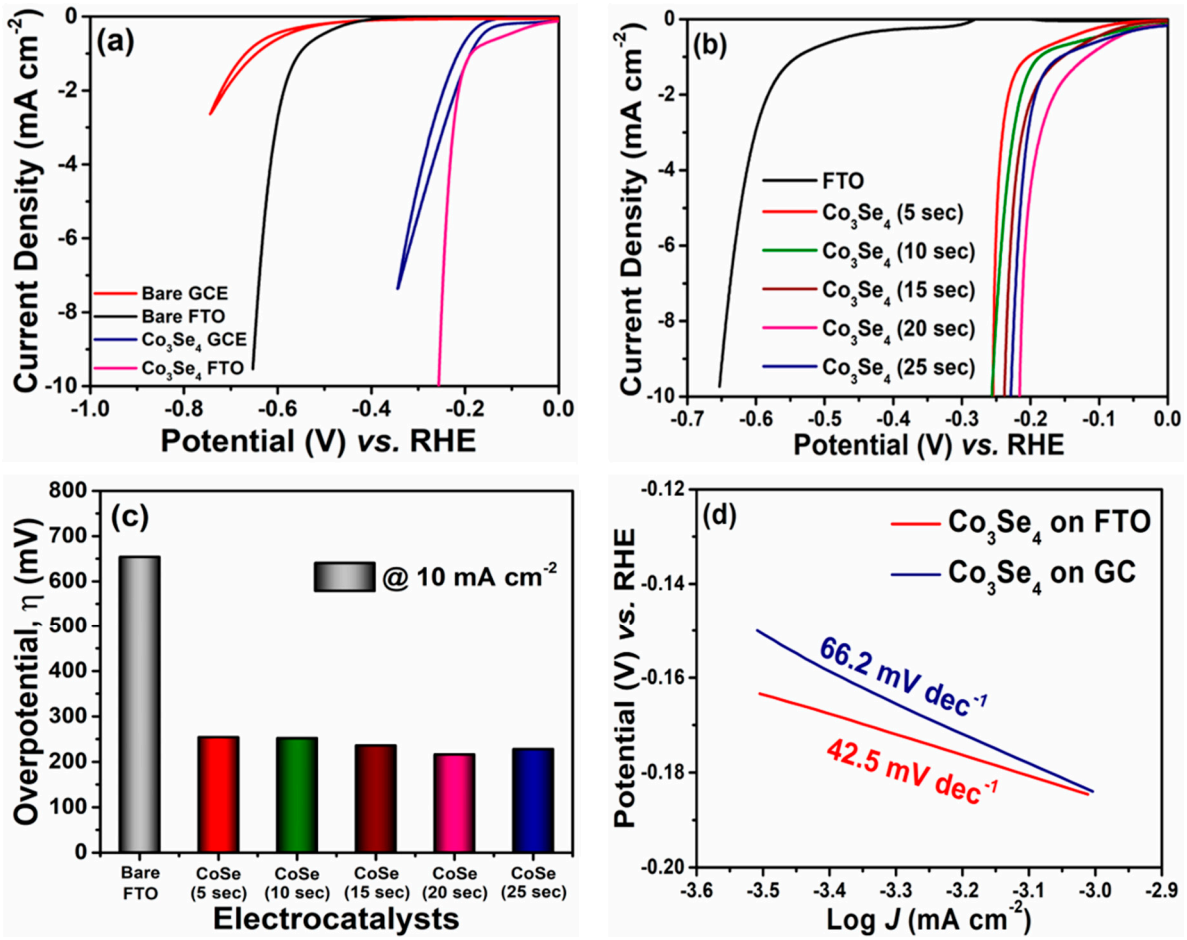


**Figure 3. Electrochemical activity with cobalt selenide ($Co_3Se_4$) deposition time on glassy carbon and FTO electrode from RDE system:** (a) Polarization curves of bare GCE, bare FTO, $Co_3Se_4$(10) on GCE, and $Co_3Se_4$(10) on FTO. (b) Polarization curves of bare FTO without any co-catalyst and FTO with cobalt selenide deposited for 5, 10, 15, 20, and 25 s. (c) HER overpotential demanded by the prepared electrocatalysts to achieve a current density of 10 mA/cm², and (d) HER Tafel slope of glassy carbon and FTO electrodeposited with cobalt selenide, as calculated from (a) and (b).

To measure the electrochemically active surface area (ECSA), the capacitance of an electrical double layer ($C_{dl}$) at a solid/electrolyte interface was evaluated by measuring the *J*–*E* response of the bare GC and $Co_3Se_4$ on GC at various scan rates, as shown in Figure 3. The $C_{dl}$ is estimated from the slope of the plot of $J_C$, which is the current at the potential with a net current density of 0 μA/cm² with increasing scan rate from 20 to 100 mV/s. The capacitance is $8.78\times10^{-3}$ μF/cm² for bare GC and 0.19 mF/cm² for $Co_3Se_4$ on GC, respectively. These values are much higher than that for a typical compact flat electrode reported to date (approximately 10–20 μF/cm²).[31] The slope is also proportional to the exchange current density, which is directly related to the catalytically active surface area.[22, 32] The ECSA is calculated from the $C_{dl}$ divided by the capacitance of a smooth planar surface of the catalyst ($C_s$). Using the general $C_s$ value of 13–17 μF/cm² in pH 0 solution (1M $HClO_4$),[33] the average ECSA of

$Co_3Se_4$ on GC and of bare GC are (2.67 and 8.91)×$10^{-5}$ $cm^2$, which corresponds to roughness factors of (13.67 and 4.55)×$10^{-4}$ $cm^2$, respectively. Therefore, $Co_3Se_4$ on GC has a large electrochemical catalytic surface area, which may also provide effective active sites for the HER.

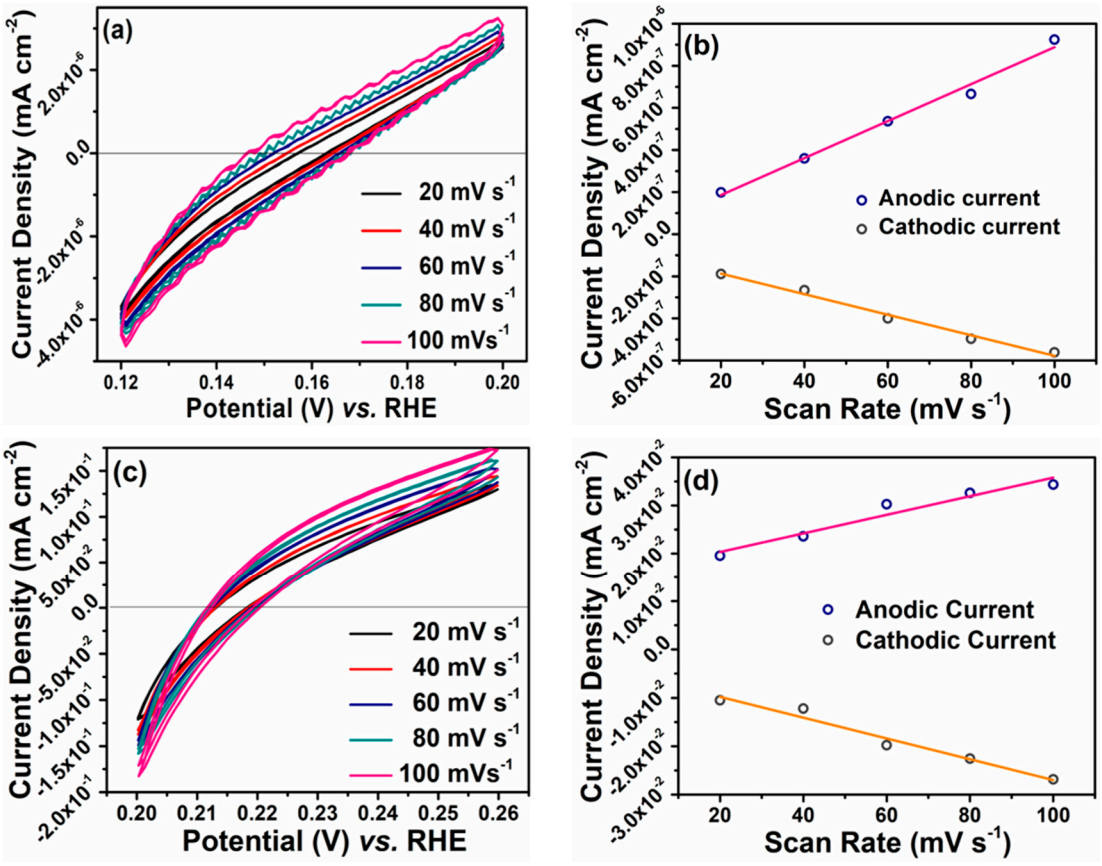


**Figure 4. The current vs potential result of** (a) Bare GC and (c) $Co_3Se_4$ on GC electrodes at different scan rates. The capacitance current ($J_C$) of (b) Bare GC and (d) $Co_3Se_4$ on GC at $J_{net}$ = 0 mA/$cm^2$ depending on scan rates. The slope of the $J_C$ to scan rates plot is the capacitance of the double layer ($C_{dl}$). (b) The value of bare GC is 8.78×$10^{-3}$ μF/$cm^2$ of cathodic current density and 4.88×$10^{-3}$ μF/$cm^2$ of anodic current density. (d) For $Co_3Se_4$ on GC, $C_{dl}$ is 0.19 mF/$cm^2$ of cathodic current density and 0.22 mF/$cm^2$ of anodic current density.

In addition, the electrodeposited $Co_3Se_4$(20) were also attempted for use as working electrodes for the water oxidation reaction. The $Co_3Se_4$(20) electrocatalyst was employed as the anode at pH 8 condition (phosphate buffer solution). Figure 4 a and b, shows the OER polarization curves of bare GC electrode, $Co_3Se_4$ deposited on GC, bare FTO, and $Co_3Se_4$ deposited on FTO, respectively. Substantially, the $Co_3Se_4$ on FTO revealed superior OER activity compared to $Co_3Se_4$ on GC, with lower onset potential (1.55 V vs RHE at 1 mA/$cm^2$) under pH 8 condition. The $Co_3Se_4$ on FTO electrocatalyst requires lower overpotential of 562 mV to attain a current density of 4 mA/$cm^2$, while the $Co_3Se_4$ on GC needed 579 mV to reach the same current density. Figure 5c differentiates the

required OER overpotential for the prepared electrocatalysts to achieve a current density of 4 mA/cm$^2$.

To recognize the rate determining step, a Tafel slope was calculated by fitting the plot to a Tafel equation ($\eta = b \log j + a$), where j represents the current density and b is the Tafel slope. Figure 5d shows the OER Tafel plot of $Co_3Se_4$ electrocatalyst on FTO and GC electrodes. A minimum Tafel slope of 103 mV/dec was obtained by the $Co_3Se_4$ electrocatalyst on FTO substrate, which implies that the rate-determining step in the electrochemical system is a single electron transfer step. Hence, the $Co_3Se_4$ catalyst electrodeposited on the FTO substrate delivered upgraded OER electrocatalytic activity. Therefore, the $Co_3Se_4$ electrocatalysts prepared by controlled deposition over the FTO and GC electrodes, act as efficient bi-functional catalysts for both hydrogen and oxygen evolution reactions.

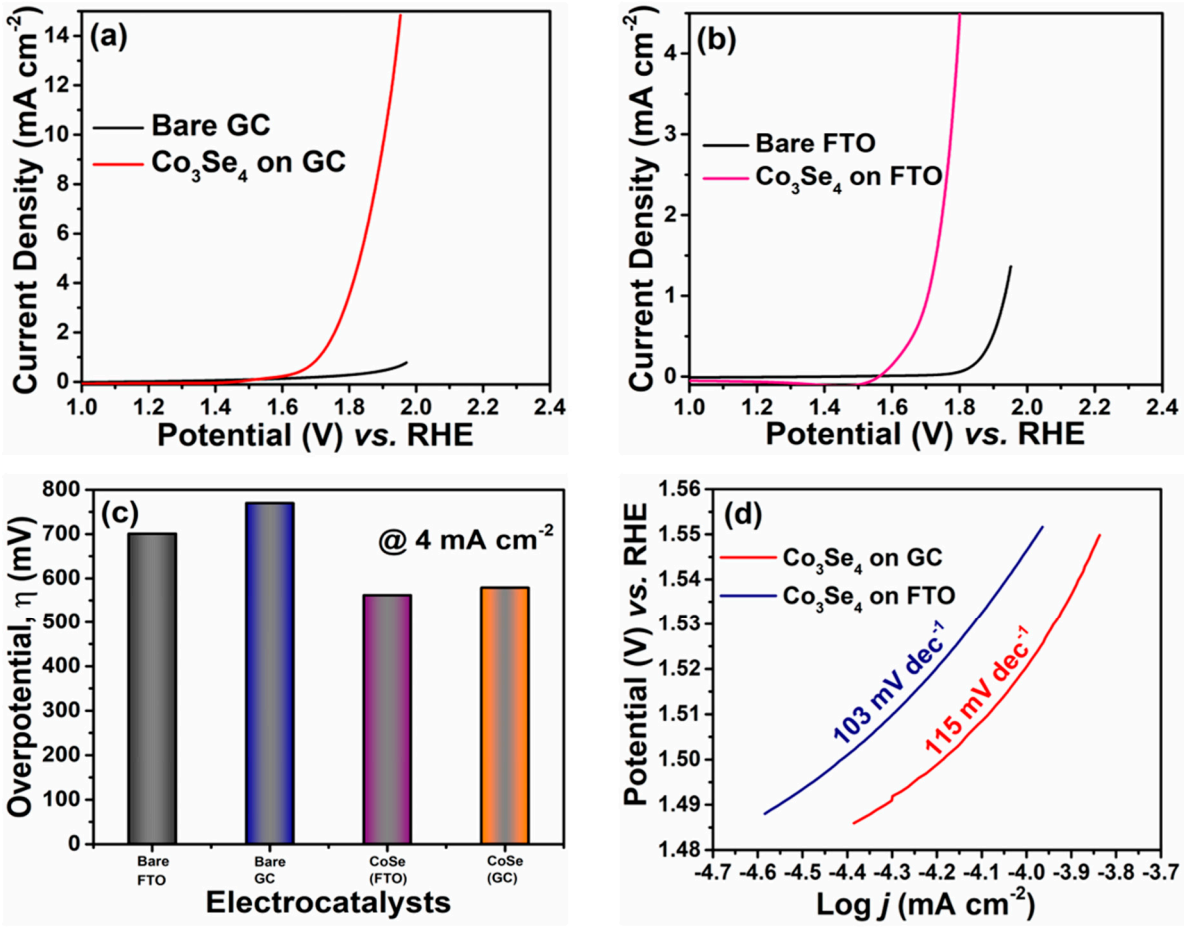


**Figure 5. OER polarization curves of $Co_3Se_4$.** (a) $Co_3Se_4$ deposited on GC and bare GC, and (b) $Co_3Se_4$ deposited on FTO and bare FTO. (c) OER overpotential demanded by the prepared electrocatalysts to achieve a current density of 4 mA/cm$^2$. (d) OER Tafel slopes of $Co_3Se_4$ deposited on FTO and GC electrodes.

## 4. Conclusions

In conclusion, we employed electrodeposited-cobalt selenide ($Co_3Se_4$) co-catalyst on a silicon photoelectrode system for the water splitting reaction. The SEM image confirms the uniform distribution of the $Co_3Se_4$ film over the electrode material. The controlled loading of $Co_3Se_4$ over the substrates was effectively optimized by varying the deposition time. The prepared $Co_3Se_4$ electrodes were successfully investigated and found to be efficient electrocatalysts for both hydrogen and oxygen evolution reactions. For the hydrogen evolution reaction, the $Co_3Se_4$ catalyst electrodeposited on FTO substrate for 20 s requires very low overpotential of 215 mV to provide an improved current density of 10 mA/cm$^2$, compared to the other prepared electrocatalysts. Moreover, this electrocatalyst yielded a very low Tafel slope value of 42.5 mV/dec. The same electrocatalyst was subjected to the oxygen evolution reaction, which required a lower overpotential of 562 mV with a reduced Tafel value of 103 mV/dec. From these enhanced HER and OER catalytic activity results, we believe that $Co_3Se_4$ prepared by this easy, one-pot electrodeposition method, seems to be the most promising candidate for commercialization as a low cost efficient electrocatalyst for water splitting.

**Author Contributions:** Conceptualization, U.S.; Methodology, U.S.; Validation, U.S.; Formal Analysis, Y.S. and S.S.; Investigation, S.S. and U.S.; Resources, U.S.; Data Curation, B.M. and S.S.; Writing-Original Draft Preparation, Y.S., J.J, and S.S.; Writing-Review & Editing, U.S., J.J., S.S. and Y.S.; Visualization, B.M. and Y.S.; Supervision, U.S.; Project Administration, U.S. ǂ These authors contributed equally to this work.

**Acknowledgments:** This research was supported by the National Research Foundation of Korea (NRF) and funded by the Ministry of Science, ICT & Future, Republic of Korea (2018R1C1B6001267 and 2018R1A5A1025224).

**Conflicts of Interest:** The authors declare no conflict of interest.

## References


1. Barber, J., Photosynthetic energy conversion: natural and artificial. *Chemical Society Reviews* **2009,** *38* (1), 185-196.
2. Walter, M. G.; Warren, E. L.; McKone, J. R.; Boettcher, S. W.; Mi, Q.; Santori, E. A.; Lewis, N. S., Solar Water Splitting Cells. *Chemical Reviews* **2010,** *110* (11), 6446-6473.
3. Zou, X.; Zhang, Y., Noble metal-free hydrogen evolution catalysts for water splitting. *Chemical Society Reviews* **2015,** *44* (15), 5148-5180.
4. Züttel, A.; Remhof, A.; Borgschulte, A.; Friedrichs, O., Hydrogen: the future energy carrier. *Philosophical Transactions of the Royal Society A: Mathematical, Physical and Engineering Sciences* **2010,** *368* (1923), 3329-3342.
5. Turner, J. A., Sustainable Hydrogen Production. *Science* **2004,** *305* (5686), 972-974.
6. Fujishima, A.; Honda, K., Electrochemical Photolysis of Water at a Semiconductor Electrode. *Nature* **1972,** *238* (5358), 37-38.
7. McKone, J. R.; Lewis, N. S.; Gray, H. B., Will Solar-Driven Water-Splitting Devices See the Light of Day? *Chemistry of Materials* **2014,** *26* (1), 407-414.
8. Chen, X.; Liu, L.; Yu, P. Y.; Mao, S. S., Increasing Solar Absorption for Photocatalysis with Black Hydrogenated Titanium Dioxide Nanocrystals. *Science* **2011**.
9. Warren, S. C.; Voïtchovsky, K.; Dotan, H.; Leroy, C. M.; Cornuz, M.; Stellacci, F.; Hébert, C.; Rothschild, A.; Grätzel, M., Identifying champion nanostructures for solar water-splitting. *Nature Materials* **2013,** *12*, 842.
10. Liao, L.; Zhang, Q.; Su, Z.; Zhao, Z.; Wang, Y.; Li, Y.; Lu, X.; Wei, D.; Feng, G.; Yu, Q.; Cai, X.; Zhao, J.; Ren, Z.; Fang, H.; Robles-Hernandez, F.; Baldelli, S.; Bao, J., Efficient solar water-splitting using a nanocrystalline CoO photocatalyst. *Nature Nanotechnology* **2013,** *9*, 69.
11. Lee, M. H.; Takei, K.; Zhang, J.; Kapadia, R.; Zheng, M.; Chen, Y.-Z.; Nah, J.; Matthews, T. S.; Chueh, Y.-L.; Ager, J. W.; Javey, A., p-Type InP Nanopillar Photocathodes for Efficient Solar-Driven Hydrogen Production. *Angewandte Chemie International Edition* **2012,** *51* (43), 10760-10764.

12. Kenney, M. J.; Gong, M.; Li, Y.; Wu, J. Z.; Feng, J.; Lanza, M.; Dai, H., High-Performance Silicon Photoanodes Passivated with Ultrathin Nickel Films for Water Oxidation. *Science* **2013,** *342* (6160), 836-840.

13. Kye, J.; Shin, M.; Lim, B.; Jang, J.-W.; Oh, I.; Hwang, S., Platinum Monolayer Electrocatalyst on Gold Nanostructures on Silicon for Photoelectrochemical Hydrogen Evolution. *ACS Nano* **2013,** *7* (7), 6017-6023.

14. Sun, K.; Pang, X.; Shen, S.; Qian, X.; Cheung, J. S.; Wang, D., Metal Oxide Composite Enabled Nanotextured Si Photoanode for Efficient Solar Driven Water Oxidation. *Nano Letters* **2013,** *13* (5), 2064-2072.

15. Powell, D. M.; Winkler, M. T.; Choi, H. J.; Simmons, C. B.; Needleman, D. B.; Buonassisi, T., Crystalline silicon photovoltaics: a cost analysis framework for determining technology pathways to reach baseload electricity costs. *Energy & Environmental Science* **2012,** *5* (3), 5874-5883.

16. Oh, I.; Kye, J.; Hwang, S., Enhanced Photoelectrochemical Hydrogen Production from Silicon Nanowire Array Photocathode. *Nano Letters* **2011,** *12* (1), 298-302.

17. Wang, X.; Peng, K.-Q.; Pan, X.-J.; Chen, X.; Yang, Y.; Li, L.; Meng, X.-M.; Zhang, W.-J.; Lee, S.-T., High-Performance Silicon Nanowire Array Photoelectrochemical Solar Cells through Surface Passivation and Modification. *Angewandte Chemie International Edition* **2011,** *50* (42), 9861-9865.

18. Strandwitz, N. C.; Comstock, D. J.; Grimm, R. L.; Nichols-Nielander, A. C.; Elam, J.; Lewis, N. S., Photoelectrochemical Behavior of n-type Si(100) Electrodes Coated with Thin Films of Manganese Oxide Grown by Atomic Layer Deposition. *The Journal of Physical Chemistry C* **2013,** *117* (10), 4931-4936.

19. Lana-Villarreal, T.; Straboni, A.; Pichon, L.; Alonso-Vante, N., Photoelectrochemical characterization of p-type silicon electrodes covered with tunnelling nitride dielectric films. *Thin Solid Films* **2007,** *515* (18), 7376-7381.

20. Peng, K.-Q.; Wang, X.; Wu, X.-L.; Lee, S.-T., Platinum Nanoparticle Decorated Silicon Nanowires for Efficient Solar Energy Conversion. *Nano Letters* **2009,** *9* (11), 3704-3709.

379 21. Faber, M. S.; Lukowski, M. A.; Ding, Q.; Kaiser, N. S.; Jin, S., Earth-Abundant Metal
380 Pyrites (FeS2, CoS2, NiS2, and Their Alloys) for Highly Efficient Hydrogen Evolution and
381 Polysulfide Reduction Electrocatalysis. *The Journal of Physical Chemistry C* **2014,** *118* (37),
382 21347-21356.
383 22. Kong, D.; Wang, H.; Lu, Z.; Cui, Y., CoSe2 Nanoparticles Grown on Carbon Fiber
384 Paper: An Efficient and Stable Electrocatalyst for Hydrogen Evolution Reaction. *Journal of*
385 *the American Chemical Society* **2014,** *136* (13), 4897-4900.
386 23. Zhang, H.; Li, Y.; Zhang, G.; Xu, T.; Wan, P.; Sun, X., A metallic CoS2 nanopyramid
387 array grown on 3D carbon fiber paper as an excellent electrocatalyst for hydrogen evolution.
388 *Journal of Materials Chemistry A* **2015,** *3* (12), 6306-6310.
389 24. Gao, M.-R.; Liang, J.-X.; Zheng, Y.-R.; Xu, Y.-F.; Jiang, J.; Gao, Q.; Li, J.; Yu, S.-H.,
390 An efficient molybdenum disulfide/cobalt diselenide hybrid catalyst for electrochemical
391 hydrogen generation. *Nature Communications* **2015,** *6*, 5982.
392 25. Zheng, Y.-R.; Gao, M.-R.; Gao, Q.; Li, H.-H.; Xu, J.; Wu, Z.-Y.; Yu, S.-H., An Efficient
393 CeO2/CoSe2 Nanobelt Composite for Electrochemical Water Oxidation. *Small* **2015,** *11* (2),
394 182-188.
395 26. Zhang, H.; Yang, B.; Wu, X.; Li, Z.; Lei, L.; Zhang, X., Polymorphic CoSe2 with Mixed
396 Orthorhombic and Cubic Phases for Highly Efficient Hydrogen Evolution Reaction. *ACS*
397 *Applied Materials & Interfaces* **2015,** *7* (3), 1772-1779.
398 27. Huang, Z.; Chen, Z.; Chen, Z.; Lv, C.; Meng, H.; Zhang, C., Ni12P5 Nanoparticles as
399 an Efficient Catalyst for Hydrogen Generation via Electrolysis and Photoelectrolysis. *ACS*
400 *Nano* **2014,** *8* (8), 8121-8129.
401 28. Bao, X.-Q.; Fatima Cerqueira, M.; Alpuim, P.; Liu, L., Silicon nanowire arrays coupled
402 with cobalt phosphide spheres as low-cost photocathodes for efficient solar hydrogen
403 evolution. *Chemical Communications* **2015,** *51* (53), 10742-10745.
404 29. Masud, J.; Swesi, A. T.; Liyanage, W. P. R.; Nath, M., Cobalt Selenide Nanostructures:
405 An Efficient Bifunctional Catalyst with High Current Density at Low Coverage. *ACS Applied*
406 *Materials & Interfaces* **2016,** *8* (27), 17292-17302.

30. Allen J. Bard, L. R. F., Electrochemical Methods: Fundamentals and Applications. *John Wiley & Sons, Inc.* **2001**, 864.

31. Randin, J. P.; Yeager, E., Differential Capacitance Study of Stress-Annealed Pyrolytic Graphite Electrodes. *Journal of The Electrochemical Society* **1971,** *118* (5), 711-714.

32. Trasatti, S.; Petrii, O. A., Real surface area measurements in electrochemistry. *Journal of Electroanalytical Chemistry* **1992,** *327* (1–2), 353-376.

33. McCrory, C. C. L.; Jung, S.; Peters, J. C.; Jaramillo, T. F., Benchmarking Heterogeneous Electrocatalysts for the Oxygen Evolution Reaction. *Journal of the American Chemical Society* **2013,** *135* (45), 16977-16987.